

In vivo micro-vascular imaging and flow cytometry in zebrafish using two-photon excited endogenous fluorescence

Yan Zeng,^{1,4} Bo Yan,^{2,4} Qiqi Sun,¹ Sicong He,¹ Jun Jiang,¹ Zilong Wen,^{2,3,5}
and Jianan Y. Qu^{1,3,*}

¹Biophotonics Research Laboratory, Department of Electronic and Computer Engineering, Hong Kong University of Science and Technology, Clear Water Bay, Kowloon, Hong Kong SAR, China

²State Key Laboratory of Molecular Neuroscience, Division of Life Science, Hong Kong University of Science and Technology, Clear Water Bay, Kowloon, Hong Kong SAR, China

³Center of Systems Biology and Human Health, School of Science and Institute for Advanced Study, Hong Kong University of Science and Technology, Clear Water Bay, Kowloon, Hong Kong SAR, China

⁴These authors contributed equally to this work

⁵zilong@ust.hk

*eequ@ust.hk

Abstract: Zebrafish has rapidly evolved as a powerful vertebrate model organism for studying human diseases. Here we first demonstrate a new label-free approach for *in vivo* imaging of microvasculature, based on the recent discovery and detailed characterization of the two-photon excited endogenous fluorescence in the blood plasma of zebrafish. In particular, three-dimensional reconstruction of the microvascular networks was achieved with the depth-resolved two-photon excitation fluorescence (TPEF) imaging. Secondly, the blood flow images, obtained by perpendicularly scanning the focal point across the blood vessel, provided accurate information for characterizing the hemodynamics of the circulatory system. The endogenous fluorescent signals of reduced nicotinamide adenine dinucleotide (NADH) enabled visualization of the circulating granulocytes (neutrophils) in the blood vessel. The development of acute sterile inflammation could be detected by the quantitative counting of circulating neutrophils. Finally, we found that by utilizing a short wavelength excitation at 650 nm, the commonly used fluorescent proteins, such as GFP and DsRed, could be efficiently excited together with the endogenous fluorophores to achieve four-color TPEF imaging of the vascular structures and blood cells. The results demonstrated that the multi-color imaging could potentially yield multiple view angles of important processes in living biological systems.

©2014 Optical Society of America

OCIS codes: (170.1470) Blood or tissue constituent monitoring; (180.4315) Nonlinear microscopy; (180.5810) Scanning microscopy.

References and links

1. R. F. Tuma, W. N. Durán, and K. Ley, *Handbook of Physiology: Microcirculation* (Elsevier, 2008).
2. J. K. Li, *Dynamics of the vascular system* (World scientific, 2004).
3. D. M. McDonald and P. L. Choyke, "Imaging of angiogenesis: From microscope to clinic," *Nat. Med.* **9**(6), 713–725 (2003).
4. D. A. Boas and A. K. Dunn, "Laser speckle contrast imaging in biomedical optics," *J. Biomed. Opt.* **15**(1), 011109 (2010).
5. I. V. Larina, S. Ivers, S. Syed, M. E. Dickinson, and K. V. Larin, "Hemodynamic measurements from individual blood cells in early mammalian embryos with Doppler swept source OCT," *Opt. Lett.* **34**(7), 986–988 (2009).
6. L. V. Wang, "Multiscale photoacoustic microscopy and computed tomography," *Nat. Photonics* **3**(9), 503–509 (2009).

7. W. Min, S. Lu, S. Chong, R. Roy, G. R. Holtom, and X. S. Xie, "Imaging chromophores with undetectable fluorescence by stimulated emission microscopy," *Nature* **461**(7267), 1105–1109 (2009).
8. G. O. Clay, A. C. Millard, C. B. Schaffer, J. Aus-der-Au, P. S. Tsai, J. A. Squier, and D. Kleinfeld, "Spectroscopy of third-harmonic generation: Evidence for resonances in model compounds and ligated hemoglobin," *J. Opt. Soc. Am. B* **23**(5), 932–950 (2006).
9. C. K. Tsai, Y. S. Chen, P. C. Wu, T. Y. Hsieh, H. W. Liu, C. Y. Yeh, W. L. Lin, J. S. Chia, and T. M. Liu, "Imaging granularity of leukocytes with third harmonic generation microscopy," *Biomed. Opt. Express* **3**(9), 2234–2243 (2012).
10. V. V. Tuchin, A. Tárnok, and V. P. Zharov, "In vivo flow cytometry: A horizon of opportunities," *Cytometry A* **79**(10), 737–745 (2011).
11. W. Zheng, D. Li, Y. Zeng, Y. Luo, and J. Y. Qu, "Two-photon excited hemoglobin fluorescence," *Biomed. Opt. Express* **2**(1), 71–79 (2011).
12. C. Li, R. K. Pastila, C. Pitsillides, J. M. Runnels, M. Puoris'haag, D. Côté, and C. P. Lin, "Imaging leukocyte trafficking in vivo with two-photon-excited endogenous tryptophan fluorescence," *Opt. Express* **18**(2), 988–999 (2010).
13. Y. Zeng, J. Xu, D. Li, L. Li, Z. Wen, and J. Y. Qu, "Label-free in vivo flow cytometry in zebrafish using two-photon autofluorescence imaging," *Opt. Lett.* **37**(13), 2490–2492 (2012).
14. O. J. Tamplin and L. I. Zon, "Fishing at the cellular level," *Nat. Methods* **7**(8), 600–601 (2010).
15. D. Li, W. Zheng, and J. Y. Qu, "Time-resolved spectroscopic imaging reveals the fundamentals of cellular NADH fluorescence," *Opt. Lett.* **33**(20), 2365–2367 (2008).
16. C. Xu and W. W. Webb, "Measurement of two-photon excitation cross sections of molecular fluorophores with data from 690 to 1050 nm," *J. Opt. Soc. Am. B* **13**(3), 481–491 (1996).
17. M. Drobizhev, N. S. Makarov, S. E. Tillo, T. E. Hughes, and A. Rebane, "Two-photon absorption properties of fluorescent proteins," *Nat. Methods* **8**(5), 393–399 (2011).
18. M. Westerfield, *The zebrafish book: a guide for the laboratory use of zebrafish (Daniorerio)* (University of Oregon Press, 2000).
19. L. Li, B. Yan, Y. Q. Shi, W. Q. Zhang, and Z. L. Wen, "Live imaging reveals differing roles of macrophages and neutrophils during zebrafish tail fin regeneration," *J. Biol. Chem.* **287**(30), 25353–25360 (2012).
20. E. R. Gillan, R. D. Christensen, Y. Suen, R. Ellis, C. van de Ven, and M. S. Cairo, "A randomized, placebo-controlled trial of recombinant human granulocyte colony-stimulating factor administration in newborn infants with presumed sepsis: Significant induction of peripheral and bone marrow neutrophilia," *Blood* **84**(5), 1427–1433 (1994).
21. Z. Lele, S. Engel, and P. H. Krone, "hsp47 and hsp70 gene expression is differentially regulated in a stress- and tissue-specific manner in zebrafish embryos," *Dev. Genet.* **21**(2), 123–133 (1997).
22. W. Zheng, Y. C. Wu, D. Li, and J. Y. Qu, "Autofluorescence of epithelial tissue: Single-photon versus two-photon excitation," *J. Biomed. Opt.* **13**(5), 054010 (2008).
23. A. V. Gore, K. Monzo, Y. R. Cha, W. Pan, and B. M. Weinstein, "Vascular development in the zebrafish," *Cold Spring Harbor Perspectives in Medicine* **2**, (2012).
24. L. Greenbaum, C. Rothmann, R. Lavie, and Z. Malik, "Green fluorescent protein photobleaching: A model for protein damage by endogenous and exogenous singlet oxygen," *Biol. Chem.* **381**(12), 1251–1258 (2000).
25. T. H. Chia, A. Williamson, D. D. Spencer, and M. J. Levene, "Multiphoton fluorescence lifetime imaging of intrinsic fluorescence in human and rat brain tissue reveals spatially distinct NADH binding," *Opt. Express* **16**(6), 4237–4249 (2008).
26. V. Kumar, A. K. Abbas, N. Fausto, and J. Aster, *Robbins and cotran: pathologic basis of disease* (Elsevier, 2009).
27. D. B. Cines, E. S. Pollak, C. A. Buck, J. Loscalzo, G. A. Zimmerman, R. P. McEver, J. S. Pober, T. M. Wick, B. A. Konkle, B. S. Schwartz, E. S. Barnathan, K. R. McCrae, B. A. Hug, A. M. Schmidt, and D. M. Stern, "Endothelial cells in physiology and in the pathophysiology of vascular disorders," *Blood* **91**(10), 3527–3561 (1998).
28. H. Jin, J. Xu, and Z. Wen, "Migratory path of definitive hematopoietic stem/progenitor cells during zebrafish development," *Blood* **109**(12), 5208–5214 (2007).
29. E. Murayama, K. Kissa, A. Zapata, E. Mordelet, V. Briolat, H. F. Lin, R. I. Handin, and P. Herbomel, "Tracing Hematopoietic Precursor Migration to Successive Hematopoietic Organs during Zebrafish Development," *Immunity* **25**(6), 963–975 (2006).
30. F. H. Martini, M. J. Timmons, and B. Tallitsch, *Human Anatomy* (Pearson Education, 2003)
31. G. E. Davis, A. N. Stratman, A. Sacharidou, and W. Koh, "Molecular basis for endothelial lumen formation and tubulogenesis during vasculogenesis and angiogenic sprouting," *International Review of Cell and Molecular Biology* **208** (2011) Chap. 3.

1. Introduction

Microvasculature, the distal function unit of the cardiovascular system, plays an important role in the fundamental activities of various organs [1,2]. Physiological structures and hemodynamics of the microvasculature system provide unique information to understand the

development of important diseases and disorders, such as inflammation, renal failure, angiogenesis of cancer, brain ischemia, blood diseases, etc. Therefore, noninvasive imaging of microcirculatory networks and the dynamics of blood cells is invaluable for the prevention, diagnosis and treatment of related diseases.

To outline the circulatory network of blood, the well established technologies of magnetic resonance imaging (MRI), positron-emission tomography (PET), computer tomography (CT) and ultrasound imaging have been used to measure the features of blood vessels, including flow velocity, blood volume and vessel permeability [3]. The major shortcomings of these imaging technologies are: (1) lack of sufficient spatial resolution for resolving individual capillaries, let alone a single blood cell; (2) many of them often involve external contrast agents to enhance image quality. In recent years, a variety of noninvasive optical imaging modalities (laser speckle imaging, Doppler optical coherence tomography, photoacoustic imaging, third harmonic generation, etc.) have also been developed for microvascular imaging. The major limitations of these techniques are that either individual blood cell cannot be clearly resolved or different types of blood cells cannot be differentiated from each other [4–10]. To overcome the limitations, label-free *in vivo* imaging of the microvasculature and blood cells trafficking in mouse and hamster models has been achieved by using two-photon excited endogenous fluorescence of tryptophan and hemoglobin [11,12]. In the zebrafish model, our previous study reported a newly discovered endogenous fluorescence signal from zebrafish blood plasma. With two-photon excited plasma and NADH fluorescence, we measured the dynamics of red and white blood cells *in vivo* [13].

Zebrafish is a powerful model organism for the study of vertebrate biology and physiology including human diseases [14]. In this study, we develop a new microvascular imaging method based on the unique fluorescence signal of blood plasma in zebrafish. The microvascular network system will be drawn out from the nearby tissue structure of endogenous fluorescence dominated by cellular NADH signals. In addition, an imaging flow cytometry is constructed and applied to measure the blood dynamics during the acute sterile inflammation, where red blood cells in the blood vessel are imaged with the negative contrast of blood plasma autofluorescence while white blood cells are identified with their cellular NADH fluorescence signals. Finally, taking advantage of short-wavelength supercontinuum emission from a photonics crystal fiber (PCF) pumped by a standard Ti:Sapphire femtosecond laser, we demonstrate four-color TPEF imaging based on the simultaneous excitation of four fluorescence molecules using a single wavelength two-photon excitation at 650 nm. The four-color images provide multiple view angles of biological activities in the living biological system. This approach can significantly reduce the complexity of multi-color imaging.

2. Materials and methods

2.1 TPEF spectroscopic imaging system

The home-built inverted TPEF spectroscopic imaging system was modified from that used in previous study [13]. The schematic diagram of the modified system is shown in Fig. 1. Briefly, the near-IR excitation source of the tunable wavelength range from 700 nm to 900 nm was generated from a standard femtosecond Ti:sapphire laser (Mira 900, Coherent). The visible short-wavelength excitation sources at 600 ± 20 nm and 650 ± 20 nm were filtered out from the broadband supercontinuum generation of a photonic crystal fiber (FemtoWHITE CARS, NKT Photonics) pumped by the femtosecond laser tuned at the short zero dispersion wavelength (775 nm). The near-IR and visible excitation light were then expanded, collimated and combined with a dichroic mirror (FF669-Di01, Semrock). An apochromatic water immersion objective lens (LD C-APO 40X, 1.15 NA, Zeiss) of 500 μm working distance was utilized to focus the excitation beam onto the samples. In order to avoid any possible tissue damage and photobleaching, the power of the short-wavelength and near-IR excitations were kept below 10 mW within the sample, respectively. We did not observe any

tissue distortion and damage in the experiments. The TPEF emissions excited at 600 nm and 650 nm were reflected by a dichroic mirror of 550 nm cutoff wavelength (T550LPXR, Chroma) and a dichroic mirror of 600 nm cutoff wavelength (T600LPXR, Chroma), respectively. The residual laser light was rejected by a short-pass filter. The TPEF signals were relayed to a circle-to-line fiber bundle that guided the signals to a spectrograph (Ocean Optics) equipped with a linear array of 16 photomultiplier tube and a time-correlated single photon counting (TCSPC) module (PML-16-C-0 and SPC-150, Becker & Hickl). This detection system provided the capability of time- and spectral-resolved measurements at each pixel of a TPEF image. The temporal and spectral resolutions of the system were about 230 ps and 13 nm of the 200 nm wavelength range, respectively. A regular TPEF image of a $90 \times 90 \mu\text{m}^2$ field of view was created by scanning a pair of galvo mirrors. The imaging depth was controlled by an actuator. The position of the zebrafish was monitored by a bright field imaging with the illumination of a white light source. A live-cell imaging chamber (Chamlide TC) was applied to maintain the temperature (28 °C) and humidity during the TPEF imaging.

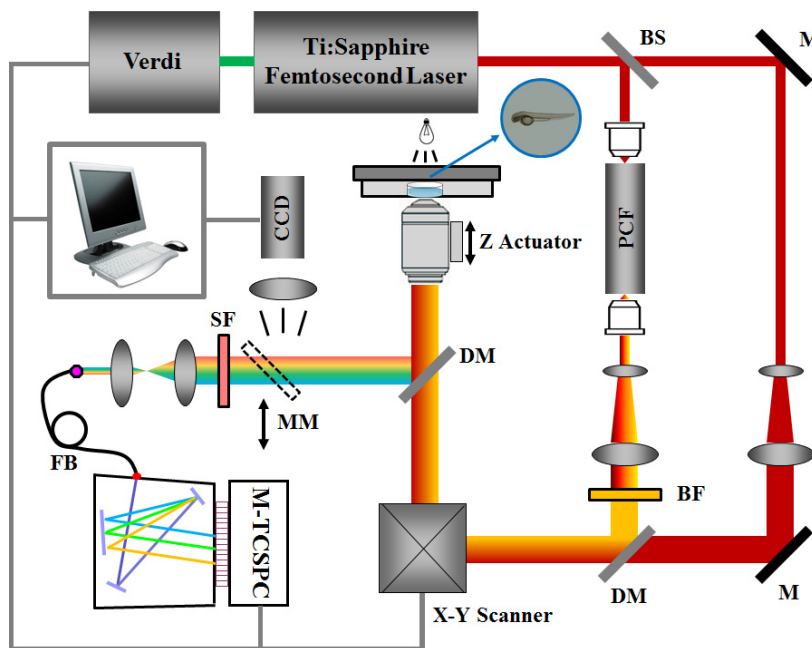


Fig. 1. Schematic diagram of the time-resolved spectroscopic imaging system. PCF: Photonic crystal fiber; BS: beam splitter; M: mirror; DM: dichroic mirror; MM: movable mirror; BF: band-pass filter; SF: short-pass filter; FB: fiber bundle; M-TCSPC: time-correlated single photon counting (TCSPC) module equipped with a multichannel PMT array

2.2 Image-guided characterization of plasma TPEF signal

We used an image-guided approach to extract the fluorescence signals of zebrafish blood plasma from the TPEF images [15]. The fluorescence spectra and time-decay under different excitation wavelengths were directly obtained from the signals at the pixels of blood plasma in the TPEF images captured by our time-resolved spectroscopic imaging system described in the previous section. The plasma TPEF signals were characterized via the verification of the two-photon excitation process, the analysis of TPEF spectral and temporal characteristics, and the measurement of the two-photon action cross-section. To confirm the two-photon excitation process, the two-photon excitation fluorescence emissions extracted from the blood vessels were measured as a function of the excitation intensity. A set of neutral density filters, mounted on a motorized filter wheel, was utilized to control the excitation power incident on the sample. The optical power of the excitation was measured by a calibrated power meter

(Model 2832-C Dual-channel power meter, Newport). The two-photon action cross section $\eta(\lambda_{ex})$ is given by the following relationship [11,16]:

$$\eta(\lambda_{ex}) = \frac{\varepsilon I_f \tau_p \lambda_{ex}^2}{P_{ave}^2}$$

where ε , I_f , τ_p , and P_{ave} are the proportional constant, measured fluorescence intensity, excitation pulse duration, and average excitation power, respectively. The pulse duration τ_p at different excitation wavelengths (600 nm, 650 nm, 720 nm, 760 nm, 800 nm) was measured using an autocorrelator (Pulsecheck-50, APE GmbH, Germany).

2.3 *In vivo micro-vascular and micro-flow imaging*

In the previous work, we discovered a significant spectral difference between blood plasma and cellular NADH TPEF signals under 650 nm excitation [13]. When the TPEF signals are collected in the wavelength range of 364 nm to 546 nm, the blood vessel of distinct plasma fluorescence peaked at 400 nm can be clearly differentiated from the surrounding tissue of signals dominated by NADH fluorescence peaked at 440 nm. To clearly differentiate the plasma signals from NADH signals in the TPEF images, we first calculated the ratio of TPEF signals at each pixel in the wavelength band from 364 to 416 nm over the signals from 429 to 481 nm, where the majority of plasma and NADH fluorescence were located, respectively. The image pixels of the microvasculature with high ratio values stood out while the image pixels of the surrounding tissue were dominated by NADH signals of low ratio values. The three-dimensional microvascular network was then reconstructed using the software: *Imaris* based on a stack of TPEF images recorded at different depths. To image the blood cell dynamics in the blood flow, the excitation focal point was scanned perpendicularly across the blood vessels with a scanning frequency of 200 Hz by using a single galvo mirror. The scanning along the blood vessel was passively achieved by the blood flow itself. Individual red blood cells can be identified with the negative contrast of blood plasma autofluorescence while the NADH signals were used to trace the circulating white blood cells [13].

2.4 *Simultaneous four-color imaging with single wavelength excitation*

Transgenic technology allows the ability to insert the genes of fluorescence proteins to animal embryos and to label specific cells and subcellular structures. It has been reported that the commonly used fluorescence proteins, including green fluorescence protein (GFP), cyan fluorescence protein (CFP) and red fluorescence protein (RFP or DsRed), can be efficiently excited at the short wavelength of 650 nm due to two-photon resonance absorption [17]. In this study, we demonstrated that the endogenous fluorescence (plasma/NADH) and fluorescence proteins (GFP/DsRed) could be excited simultaneously at 650 nm and their fluorescence signals could be differentiated clearly by our spectroscopic imaging system. We coded the TPEF spectral signals in different wavelength bands into different colors to visualize the white blood cells (neutrophil or macrophage) labeled with fluorescence proteins (signals in the wavelength band of 494 nm to 520 nm were coded in green for GFP while signals in the wavelength band of 546 nm to 559 nm were coded in purple for DsRed). For the vascular structures, the circulatory networks of blood plasma signals in the wavelength band of 364 nm to 416 nm were coded in yellow and the signals of endothelia, dominated by NADH in the wavelength band of 429 nm to 481 nm were coded in blue. It should be emphasized that due to the strong two-photon resonance absorption of DsRed, only the left shoulder of the DsRed fluorescence was collected to form TPEF image [13, 17].

2.5 Animal model

The wild-type line, strains AB and the transgenic line, *Tg(lyz:DsRed2)* (neutrophil is labeled by DsRed) and *Tg(corola:eGFP,lyz:DsRed2)* (neutrophil is double labeled by DsRed and GFP while macrophage is labeled by GFP), were raised under standard conditions [18,19]. Embryos were maintained in egg water containing 0.2 mM N-phenylthiourea (PTU, Sigma) to prevent pigment formation. To study the immune response to acute sterile inflammation, strains AB and *Tg(lyz:DsRed2)* were injected with heat shock promoter drive pro-inflammatory cytokine to induce the acute sterile inflammation [20]. These embryos and control embryos injected with H₂O were raised at 26°C for 3 days to reduce basal activation of the heat shock promoter [21]. Heat shock treatment was carried out at 39°C for 2 × 2 hours with the 1-hour interval. The experiment started 12 hours post heat shock treatment. All embryos were mounted in 1% low melting agarose with 0.02% tricaine and 0.2 mM N-phenylthiourea.

3. Results and discussions

3.1 Two-photon excitation fluorescence characteristics of zebrafish plasma

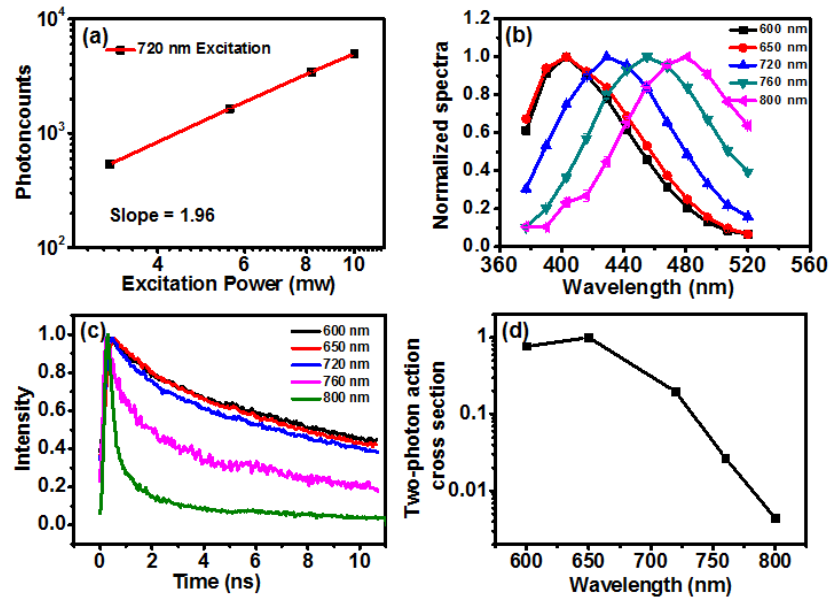


Fig. 2. Two-photon excitation fluorescence characteristics of zebrafish plasma. (a) TPEF intensity as a function of excitation power at the wavelength of 720 nm; (b) TPEF spectra excited at different wavelengths; (c) TPEF decays excited at different wavelengths; (d) two-photon action cross-sections of plasma fluorescence at different excitation wavelengths.

We first characterized the two-photon excitation fluorescence of zebrafish plasma in the dorsal vein and artery. Figure 2(a) shows the plasma fluorescence intensity as a function of excitation power at 720 nm in logarithmic coordinates. Linear fitting gives a slope equal to 1.96, confirming the fluorescent process of two-photon absorption. Similar results were also found at other excitation wavelength, such as 600 nm, 650 nm, 760 nm, and 800 nm (data not shown), indicating that the fluorescent compound in blood plasma is unlikely to have significant single-photon absorption in the wavelength range of 600 nm to 800 nm. The results of the fluorescence spectra and fluorescence lifetime measurement are displayed in Fig. 2(b) and 2(c), respectively. Under 600 nm or 650 nm excitation, the fluorescence spectra peaked at ~400 nm, and the fluorescence lifetime decay is almost identical. A significant spectral red shift can be observed with the increase of the excitation wavelength, similar to

the other large fluorescent molecules with complex energy states such as collagen and keratin [22]. In addition, a rapid decay of fluorescence lifetime was recorded when the excitation wavelength was tuned longer (>800 nm). The two-photon action cross section (in Fig. 2(d)) shows that much higher two-photon absorption occurs in short excitation wavelength such as at 600 nm or 650 nm. The excitation efficiency at 800 nm drops significantly and is about ~ 200 times lower compared to the excitation efficiency in short wavelength. Therefore, to effectively image the vascular structure using the plasma TPEF signal, the excitation wavelength should be not over 720 nm to be able to achieve high excitation efficiency. In future study, a biochemical investigation will be carried out to identify the fluorescent compound(s) in the zebrafish plasma because such strong blood plasma autofluorescence has not been found in other higher animals such as mice, rabbits and humans (data not shown).

3.2 Microvasculature imaging based on endogenous NADH and plasma fluorescence

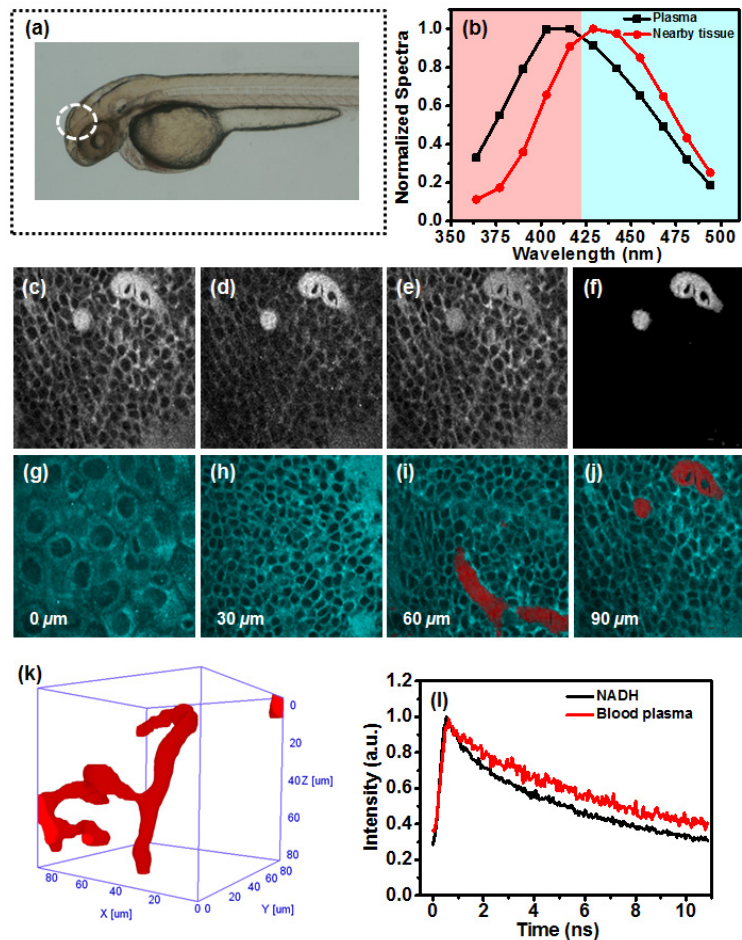


Fig. 3. Microvasculature imaging of zebrafish brain. (a) The location of the TPEF measurement in the brain; (b) TPEF spectra of the blood plasma and the brain tissue excited at 650nm; (c)-(f) Ratio imaging for microvascular vessel extraction; (c)-(e) TPEF images formed with the signals in the wavelength band of 364-481 nm, 364-416 nm, and 429-481 nm, respectively; (f) Ratio image by dividing (d) over (e). (g)-(j) TPEF images at different depths (detailed depth-resolved TPEF images are shown in [Media 1](#)); (k) three-dimensionally reconstructed microvascular network in the brain (see detail in [Media 2](#)); (l) lifetime decays of blood plasma and brain tissue TPEF signals; Image size: $90 \mu\text{m} \times 90 \mu\text{m}$.

The zebrafish brain (Fig. 3(a)) of fine and complex microvascular networks was chosen to study the microvasculature imaging based on endogenous TPEF signals from plasma and tissue. As shown in Fig. 3(b), under short wavelength excitation (650 nm), the plasma emits 400 nm peaked fluorescence of significant blue-shift from the cellular NADH fluorescence peaked at ~440 nm of the surrounding brain tissue. Therefore, the microvasculature featured by the plasma fluorescence can be extracted. The details are shown in Fig. 3(c)-3(f). In particular, Fig. 3(c)-3(e) shows the raw TPEF images formed with the signals in the wavelength bands of 364-481 nm, 364-416 nm and 429-481 nm, respectively. The ratio image (Fig. 3(f)) for extracting microvasculature was then calculated by dividing 361-416 nm band image over 429-481 nm band image. The pixels of blood plasma with high ratio value were coded in red while the pixels dominant by NADH signals were coded in cyan. Figure 3(g)-3(j) displays a set of representative TPEF images taken from the brain of the zebrafish at different depths. As can be seen, a thin layer of epithelium cells was located in the upper layer of the brain (Fig. 3(g)), followed by underlying tissue of tightly connected neural cells and microvascular vessels (Fig. 3(h)-3(j)). The microvasculature is visualized with the contrast between plasma and NADH fluorescence when the imaging depth is over 50 μm below the brain surface. Figure 3(k) displays a representative three-dimensional (3D) image of the zebrafish brain reconstructed from a stack of depth-resolved images. The results demonstrate that the label-free 3D microvasculature imaging approach is able to provide unique information to reveal the fine structure of the microvascular network. To study dynamic process of microvascular function, much faster imaging speed and reconstruction are required. By replacing the spectrograph based detection system with two single channel PMTs to collect TPEF signals in two wavelength bands, respectively, we can significantly improve signal to noise ratio under the same excitation condition and achieve much higher imaging speed. In general, this imaging capability is particularly important in the study of vascular functions and vascular system development as well as many vasculature related diseases. For example, cranial vessel formation is important to study both the development of central nervous system and cerebrovascular pathologies, such as stroke and cerebral hemorrhage. Vascular sprouting and intersegmental vessel patterning are associated with the neuronal expressed receptors for guidance molecules such as Semaphorins, Netrins, and Ephrins [23]. In addition to imaging microvascular structures, the spectral and time-resolved NADH fluorescence signals from the surrounding brain tissue also provide information on cellular energy metabolism. In particular, the ratio of NADH in free form over protein-bound form and the fluorescence lifetime of NADH are sensitive metabolic indicators [15]. Compared with the commonly used fluorescent protein labeling technique, the label-free technology can reduce the complexity of transgenic technology and the risk of introducing large fluorescent protein molecules that may interfere with the normal functions of the biological system [24]. Finally, we found that though the plasma fluorescence has the long lifetime, the fluorescence of the NADH signals in zebrafish is substantially longer than those reported from the study of cells, other animal models and human subjects [15, 25]. As shown in Fig. 3(l), the NADH fluorescence lifetime is only slightly shorter than the plasma fluorescence, meaning that two signals cannot be differentiated from each other in the time domain. The exact mechanism causing the long lifetime of NADH fluorescence in zebrafish is unknown.

3.3 Imaging of circulating neutrophils in the development of acute sterile inflammation

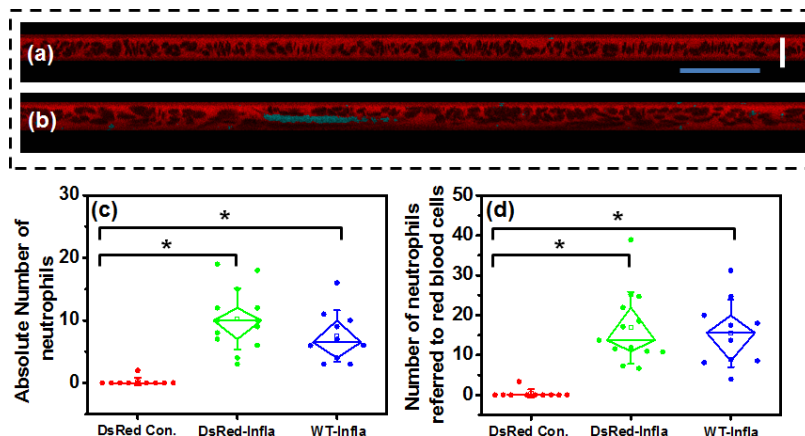


Fig. 4. *In vivo* TPEF imaging cytometric detection of acute sterile inflammation (a) blood flow TPEF image of control zebrafish (*Tg(lyz:DsRed2)*); (b) blood flow TPEF image of control zebrafish (strain AB) with acute sterile inflammation; (c) absolute counting number of circulating neutrophils in control zebrafish embryo (*Tg(lyz:DsRed2)*) and zebrafish embryo (*Tg(lyz:DsRed2)*) and strain AB with induced acute sterile inflammation; (d) the counting number of circulating neutrophils normalized to circulating erythrocytes. Scale bars for all the flow images are shown in (a): vertical (spatial scale), 25 μm ; horizontal (temporal scale), 1s; * indicates t-test p value $\ll 0.05$.

To induce the acute sterile inflammation, the heat shock promoter was first injected into the eggs of the zebrafish strains. Over-expression of pro-inflammatory cytokine after heat shock resulted in acute sterile inflammation [20]. Figure 4(a) shows the typical blood flow image captured in zebrafish embryo (*Tg(lyz:DsRed2)*) with the injection of water as control. Individual flowing red blood cells can be clearly resolved by the negative contrast over the bright plasma autofluorescence. Figure 4(b) shows a typical blood flow image with a rolling neutrophil formed with NADH signals (coded in cyan). In general, rare circulating neutrophils, verified by the blood flow image formed with DsRed fluorescence signals, were found in the blood vessels of the control fish [13]. However, the number of circulating neutrophils increased significantly in the blood flow of the zebrafish embryo after acute sterile inflammation was induced. To quantify the circulating neutrophils in the blood flow before and after acute sterile inflammation, we counted their numbers in the blood flow images recorded within period of 3 minutes. The box charts of the counting results are shown in Fig. 4(c). As can be seen, the number of circulating neutrophils increased significantly in the fish with acute sterile inflammation, indicating that the counting of circulating leukocytes can be used as an *in vivo* cytometer to assess acute inflammation. This *in vivo* cell counting capability could potentially be used in the study of other important diseases, such as leukemia, cancer and allergy [26]. However, it should be emphasized that the counted number of circulating neutrophils is a function of blood flow velocity and the size of the blood vessel. A calibration is critical to accurate monitoring of the change of cells in the whole circulation system. It is known that the red blood cells filling microvascular lumen is a good indicator of the blood flow characteristics and the blood vessel geometry. Because the number of red blood cells in the flow image can be accurately counted, we used the red blood cell count as the reference for the calibration of the circulating neutrophil counting. In principle, dividing the absolute number of circulating neutrophils by the corresponding number of red blood cells in the blood flow images recorded over the certain period of time, the errors caused by the variations of blood flow velocity and blood vessel size could be calibrated. Figure 4(d)

displays the calibration results of the circulating neutrophil count per 10,000 red blood cells in the blood stream.

3.4 Simultaneous four-color imaging of blood cells and vascular structures

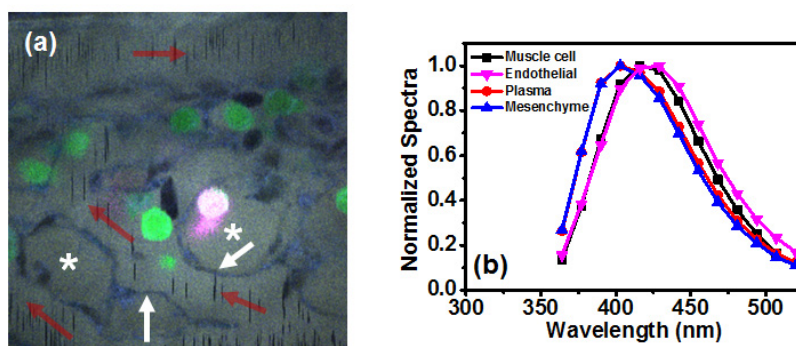


Fig. 5. Simultaneous four-color imaging with single excitation wavelength. (a) color coded TPEF image taken in the blood island (red arrow indicates the direction of blood flow; the image size: $90 \mu\text{m} \times 90 \mu\text{m}$); (b) The measured fluorescence spectra of muscle cells, endothelial cells, blood plasma and mesenchyme under 650 nm two-photon excitation.

Interactions such as those between blood cells and vascular endothelial cells and red cells and monocytes/macrophages are important scientific topics [27]. For example, the process of leukocyte recruitment to the tissue sites of inflammation involves direct cell-to-cell interactions between leukocytes and vascular endothelial cells. The interactions between red blood cells and endothelial cells have the significant influence on the microcirculatory flow under normal and pathological conditions. The study of these interactions requires an imaging system to produce the images of various blood cells and endothelial cells simultaneously. In this work, we chose the posterior blood island (PBI) of zebrafish to demonstrate the capability of simultaneous TPEF imaging of multiple blood cells and microvascular structures using single excitation. The rich microvascular structure and various mature blood cells can be found at PBI that acts as an intermediate hematopoietic organ between the caudal artery and caudal vein [28–30]. As shown in Fig. 5(a), by using short wavelength two-photon excitation (650 nm) and spectroscopic imaging, we were able to simultaneously image leukocytes (neutrophils and macrophages) labeled with fluorescent proteins (GFP/DsRed), endothelial cells with endogenous NADH signals, and microvasculature with endogenous plasma signals. The key biological features of the PBI, including the branching of caudal veins, mature blood cells and mesenchymal cells producing blood plasma, can be clearly identified. In detail, we used imaging guided spectroscopic analysis to extract the TPEF spectra of plasma, mesenchyme, endothelium and surrounding muscles [15]. As can be seen in Fig. 5(b), the TPEF signals of the endothelium and surrounding muscles are dominated by NADH fluorescence and the signals from the mesenchyme are identical to plasma fluorescence. In Fig. 5(a), the fast moving red blood cells (dark lines) can be easily identified in the microvascular vessels. The image of a red blood cell collapsed into a line because the image acquisition time was 16 seconds and not sufficiently fast to capture the image of individual red blood cells. Therefore, the structures of the blood vessels are marked with dark lines, the distorted images of flowing red blood cells. The resting leukocytes of round shapes are macrophages labeled with GFP and neutrophils labeled with both GFP/DsRed, respectively. A thin layer of endothelial cells (pointed out by white arrows), forming the lumen of the blood vessel, identified with the circulating red blood cells (dark lines in Fig. 5(a)) [31], are visualized by cellular NADH signals coded in blue. The mesenchyme (labeled with the asterisk) located in the regions among the blood vessels has identical fluorescence

characteristics to blood plasma, where the plasma proteins are synthesized by mesenchymal cells [30].

4. Conclusion

In this study, we have developed a new methodology for *in vivo* micro-vascular and micro-flow imaging by using two-photon excitation endogenous fluorescence in zebrafish. The 3D structures of fine microvascular networks in the brain were reconstructed based on the unique spectral characteristics of blood plasma TPEF signals. We demonstrated that imaging flow cytometry provides the quantitative counting of circulating blood cells, which could be used for *in vivo* monitoring the disease development and treatment, such as acute sterile inflammation. In addition, the calibrated counting of circulating leukocytes (neutrophils) in blood vessels of different flow velocity and size could potentially improve the accuracy of measurement of circulating cells in the whole circulation system. Finally, using a single wavelength excitation at 650 nm and spectroscopic detection, we achieved simultaneous four-color imaging of multiple blood cells and vascular structures. This imaging capability could potentially be used to address important biological topics such as the interactions between blood cells and vascular endothelial cells and red cells and monocytes/macrophages.

Acknowledgments

This work was supported by the Hong Kong Research Grants Council through grants 662513, N_HKUST631/11, T13-607/12R and T13-706/11-1, AOE/M-09/12, and HKUST through grant RPC10EG33.